Investigation of H_2 formation in electron-impact double ionization and fragmentation of tetrahydrofuran by multiparticle coincidence momentum imaging and *ab initio* calculations

Shaokui Jia, Jiaqi Zhou,* Chenkai Zhang, Tao Yang,† Jianzhi Xu, Xiaorui Xue, Xintai Hao, Qingrui Zeng, and Xueguang Ren‡

MOE Key Laboratory for Nonequilibrium Synthesis and Modulation of Condensed Matter, School of Physics, Xi'an Jiaotong University, Xi'an 710049, China

(Received 25 February 2024; accepted 8 May 2024; published 22 May 2024)

We report the fragmentation dynamics of double ionization of tetrahydrofuran (THF) induced by electron impact ($E_0 = 200$ eV). Using a multiparticle coincidence momentum spectrometer, the hydrogen molecule (H_2) production channel, i.e., double ionization and fragmentation of $THF^{++} \rightarrow H_2 + C_3H_5^+ + CHO^+$, is observed and identified using an ion-ion coincidence map and the correlated projectile energy-loss spectrum. The measured kinetic energy release, combined with *ab initio* molecular-dynamics simulations and high-level potential energy surface (PES) calculations, reveals the detailed fragmentation dynamics of the H_2 production channel. From the measured energy-loss spectrum, we determine the initial ionization mechanism of the fragmentation channel as a double-ionization excited state (3.3 eV above the ground state). The PES calculations reveal several H_2 formation pathways, which are all below the energy of the excited state and hence can proceed barrierless. We find that the H_2 formation and ejection occur on an ultrafast timescale (approximately 50 fs), which is followed by ring opening via the C–O bond cleavage and ultimate Coulomb explosion. The present observation of the state-resolved fragmentation mechanism and dynamics is expected to provide valuable insights into the formation process of hydrogen molecules in the interstellar medium, as well as hydrogen storage and production.

DOI: 10.1103/PhysRevA.109.052821

I. INTRODUCTION

Ionization and fragmentation of molecules induced by high-energy radiation and electron and ion impact are fundamental physical phenomena. The breaking and rearrangement of chemical bonds during fragmentation processes can lead to the formation of unexpected fragments, which holds significant implications for our understanding of the origins of many noteworthy molecules. For instance, the interest in the hydrogen molecule (H_2) has been rewarded due to its significance in the interstellar medium (ISM) [1] and clean energy resources [2]. Hydrogen molecules are produced typically through two pathways: One involves the collision and combination of two neutral hydrogen atoms and the other entails the dehydrogenation reaction of hydrogen-rich molecules. In the latter case, two or even more chemical bonds binding hydrogen atoms are broken and a new chemical bond is formed between two hydrogen atoms. This poses substantial challenges for studying the dynamic aspects of hydrogen molecule formation.

In recent years, advancements in experimental techniques have enabled comprehensive characterization of H_2 formation dynamics through kinematically complete experiments, in which the three-dimensional (3D) momentum vectors of all-final-state products are determined. This has allowed for the study of H_2 formation and roaming mechanisms in many hydrogen-rich molecules. The H_2 molecule formed by molecular isomerization (e.g., hydrogen migration) can roam around the remaining molecular moiety and capture a proton to form H_3^+ [3–7]. In parallel with proton capture, electron transfer between H_2 and the remaining fragment forms the H_2^+ ion, known as the inverse harpoon mechanism [8–10]. Pump-probe experiments show that these processes proceed on an ultrafast femtosecond timescale [6,8–10]. As the hydrogen molecule acquires high kinetic energy during the dissociation process, the shallow potential barrier cannot confine it, resulting in the failure of roaming and the dissociation of the hydrogen molecule [11–18]. However, our understanding of neutral H_2 formation mechanisms including the initial electronic states, key transition states, and dissociation dynamics remains incomplete.

In this work we report the formation mechanism and dynamics of the H_2 molecule in doubly ionized tetrahydrofuran (THF) (C_4H_8O) induced by electron impact. The THF molecule is a hydrogen-rich five-membered ring molecule featuring one oxygen heteroatom and four (CH_2) units, which also serves as a crucial analog to the DNA backbone. In light of its significance in biochemistry, THF has been studied intensively as a prototypal system for the sugar-ring structure in DNA, particularly in investigations of the ionization and subsequent fragmentation dynamics using electron impact [19–30], carbon ion collision [31], and light radiation [32–34]. The abundant H atoms in the THF molecule also provide the prerequisites and advantages for the generation of H_2 molecules. Here we identify the H_2 molecule production channel $H_2 + C_3H_5^+ + CHO^+$ using a multiparticle

*zhoujiaqi@xjtu.edu.cn
†taoyang1@xjtu.edu.cn
‡renxueguang@xjtu.edu.cn

coincidence momentum spectrometer. Two product ions and one electron are measured in triple coincidence and the 3D momentum vector of each particle is determined. Consequently, the projectile energy-loss E_{loss} spectrum and kinetic energy release (KER) spectrum are obtained, which enable us to reveal the ionization and fragmentation details of the H_2 formation channel. Through the combination of the *ab initio* molecular-dynamics (AIMD) simulations and potential energy surface (PES) calculations, the molecular hydrogen formation channel is revealed to proceed via H_2 formation and ejection on an ultrafast timescale (approximately 50 fs), followed by the ring opening via the C–O bond cleavage, and Coulomb explosion for formation of the final ionic fragments ($C_3H_5^+ + CHO^+$).

II. EXPERIMENTAL METHODS

The experiment is performed using a multiparticle coincidence momentum imaging spectrometer (reaction microscope), which was introduced comprehensively in previous studies [35–38]. In general, a pulsed electron beam crosses perpendicularly a supersonic cold gas jet, and the final-state electrons and ions produced in the collision process are extracted separately to two position- and time-sensitive detectors. The projectile electron is produced by a photoemission electron gun equipped with a tantalum photocathode that is irradiated by UV-light pulses ($\lambda = 266$ nm, $\Delta t = 0.5$ ns). The THF vapor carried by helium gas (1 bar) undergoes supersonic expansion into the reaction chamber and intersects the electron beam. A homogeneous electric field (approximately 1 V/cm) and magnetic field (approximately 7 G) guide the electrons onto microchannel plate detectors with delay-line position readout. The scattered electrons at small scattering angles in the near forward direction can be detected completely [38]. Since the fragment ions carry typically higher momenta, achieving 4π collection of ions requires a higher electric field (approximately 25 V/cm). This is obtained through a pulsed-field generator after the electron extraction. Two-dimensional positions and times of flight (TOFs) of charged particles can be recorded in the list mode during the experiments. Finally, the initial momentum vectors, and consequently the kinetic energies of the electrons and ions, are reconstructed in the offline analysis.

III. THEORETICAL CALCULATIONS

To understand the fragmentation dynamics of the THF^{2+} dication, we performed AIMD simulations by using the extended Lagrangian molecular-dynamics scheme adopting the so-called atom-centered density-matrix propagation method [39–41]. This method enables the extended Lagrangian approach to molecular dynamics with accurate long-term energy conservation using Gaussian basis functions and propagating the density matrix, which were calculated with the B3LYP/cc-pVDZ method. Each step was set to 0.5 fs with a total simulation time of 1.0 ps. Initially, the molecular geometries and velocities of each atom in the neutral THF were sampled using the quasiclassical fixed normal-mode sampling method. This process was conducted at a temperature of approximately 30 K, where the populations of the initial rovibrational states were determined based on Boltzmann distributions. In the simulations, we induced the Coulomb explosion of the electronically excited state of THF^{2+} by introducing an internal energy of 0.3 hartree into the electronic ground state of the system. This approach provides an approximate consideration of the electronically excited state in our calculations [42]. The surplus excited energy undergoes conversion into the vibrational energy of the molecule through rapid internal processes, ultimately leading to dissociation.

To elucidate the PES of the dissociation channels, the intermediate states and transition states (TSs) encountered in the channels were calculated using a B3LYP functional and an aug-cc-pVTZ basis set. Frequency calculations were carried out at the same level of theory to confirm that all the optimized structures are local minima for intermediate states or have one (and only one) imaginary frequency for TSs. The reaction path connections between intermediate and transition states were further confirmed by the intrinsic reaction coordinate calculations [43]. For a comprehensive evaluation of the energy of every intermediate state, single-point-energy calculations using the coupled-cluster with single and double and perturbative triple excitations method with the basis set aug-cc-pVTZ were performed using B3LYP–aug-cc-pVTZ optimized geometries. The reported energies here have been corrected by the zero-point-energy calculations at the B3LYP–aug-cc-pVTZ level. All the above PES calculations and AIMD simulations were conducted using a GAUSSIAN package [44]. There are two conformers for the THF molecule, C_2 (twisted) and C_s (envelope). The C_2 conformer is most stable and predominant for the target THF molecule under the current experimental condition [30]. Thus, the following discussion focuses on the C_2 symmetry of THF.

IV. RESULTS AND DISCUSSION

The reaction channels in electron-impact ionization of THF are identified by the TOF correlation map between two detected fragment ions, as shown in Fig. 1. The mass-to-charge ratios corresponding to the TOF at the centers of coincidence lines are used to identify the ion species in the reaction channels. Simultaneously, a native frame method is employed to determine the reaction channels and to further eliminate the effects of overlaps from the other dissociation channels [45]. Two sharp coincidence lines are created by the typical two-body Coulomb explosion (CE) channels of $C_2H_4^+ + C_2H_4O^+$ and $CH_2O^+ + C_3H_6^+$, respectively. The shapes of coincidence lines originate from the back-to-back emission of two fragments with equal momentum magnitudes. The H_2-loss H_2 (or 2H) $+ C_3H_5^+ + CHO^+$ and 3H-loss $3H + C_3H_4^+ + CHO^+$ channels have also been observed in the experiment. The broad correlation feature for the H_2-loss channel is caused by the missing momenta of the undetected neutral species. Among all dissociation channels, the H_2 (or 2H) $+ C_3H_5^+ + CHO^+$ channel is attractive, as it involves the loss of two hydrogen atoms and the dissociative mechanism is not clearly defined. The two undetected hydrogen atoms are determined to form molecular hydrogen H_2 through theoretical calculations, as detailed in the following discussion.

In our measurement, two fragment ions and one outgoing electron are detected in coincidence. Thus, we can obtain the

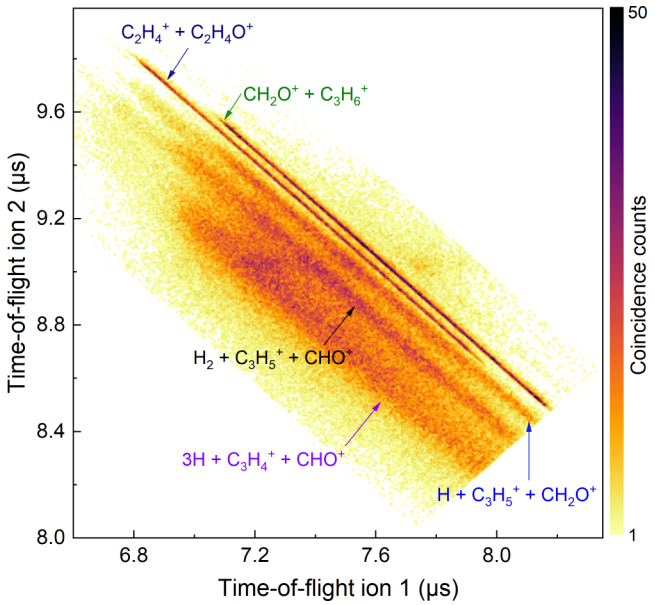

FIG. 1. Correlation of the time of flight of the two detected ions. Several reaction channels from dissociation of the THF^{2+} dication can be identified, including the complete two-body Coulomb explosion ($C_2H_4^+ + C_2H_4O^+$ and $CH_2O^+ + C_3H_6^+$), H-loss ($H + C_3H_5^+ + CH_2O^+$), H_2-loss ($H_2 + C_3H_5^+ + CHO^+$), and 3H-loss ($3H + C_3H_4^+ + CHO^+$) dissociation channels. The color bar is linear and represents the number of measured coincidence counts.

projectile energy-loss E_{loss} spectrum associated with the H_2 formation channel, which allows us to determine the initial ionization state of the dissociation process. The projectile energy loss is defined as the incident projectile energy E_0 minus the scattered electron energy E_1 ($E_{loss} = E_0 - E_1$). The energy-loss spectrum of $H_2 + C_3H_5^+ + CHO^+$ channel is displayed in Fig. 2. The onset of the E_{loss} spectrum is determined as approximately 30.8 eV (refer to the vertical dashed line

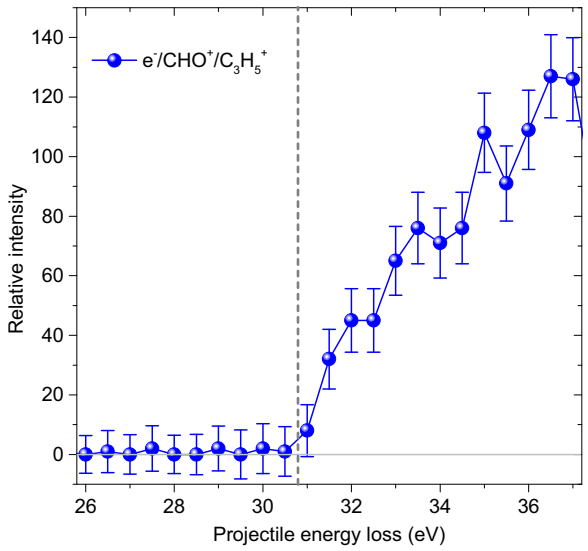

FIG. 2. Projectile energy-loss spectrum for the H_2 formation channel $H_2 + C_3H_5^+ + CHO^+$. The vertical dashed line represents the onset of the H_2 formation channel.

in Fig. 2), which is lying above the double-ionization (DI) threshold of THF (27.5 eV) [27]. This result indicates that the H_2 formation channel is initiated when the THF^{2+} dication is populated in the excited state, elevated by 3.3 eV compared to the ground state (ionization of two outermost valence electrons). The attraction between the dipolar H_2 and $C_4H_6O^{2+}$ cation could lead to the formation of metastable $H_2 - C_4H_6O^{2+}$ complexes, in which the H_2 remains weakly bound with the remaining cations. Thus, H_2 molecule ejection cannot occur directly if the kinetic energy of H_2 is not high enough to overcome the barrier. In this case, the roaming H_2 molecule can capture a proton from the remaining moiety or transfer an electron to it, leading to the formation of H_3^+ or H_2^+, which has been discussed in previous studies [5,7,8]. The excess energy allows the dications to occupy high vibrational states through internal energy conversion, facilitating H_2 formation and fragmentation from the THF^{2+} dication.

The DI excited states can be accessed by directly ionizing two outer-valence electrons or ionizing one inner-valence electron followed by the Auger process. The inner-valence molecular orbitals for the THF molecule, including 6*a*, 4*b*, 3*b*, 5*a*, and 4*a*, are feasible for triggering Auger processes, whereas *K*-shell ionization is excluded in the present experiment due to energy limitations of the incident electrons (200 eV). Based on the reported binding energy spectrum and measured E_{loss} spectrum of THF [46–48], the initial electronic state is deduced. The candidate inner-valence orbital, namely 4*a*, is mainly composed of C 2*s* and O 2*s* orbitals with energies from 19.0 to 32.0 eV [20,27]. The ionization energy of the C $2s^{-1}$ state ranges from 19.0 to 24.6 eV, which lies below the double-ionization threshold of THF (27.5 eV). The ionization of the O 2*s* orbital shows a broad binding energy band located at around 31.8 eV, suggesting that the removal of an O 2*s* electron could lead to various ionization states lying above the double-ionization threshold. Thus, the excited THF dication can be formed by ionizing an O 2*s* electron, followed by Auger decay with one outer-valence electron filling the inner-valence hole and another outer-valence electron emitting from the molecule.

The momentum vectors and corresponding kinetic energies of two charged particles $C_3H_5^+ + CHO^+$ are determined from the measured TOFs and positions of the particles hitting the detectors. The momentum of the lost H_2 is derived from the momenta of the two cations, ensuring the total momentum conservation. The KER of the $H_2 + C_3H_5^+ + CHO^+$ channel is obtained and shown in Fig. 3(a), which shows a single peak at about 5.0 eV. To further unveil the details of molecular-dynamics evolution, we carried out the AIMD simulations, which started by introducing an internal energy into the ground state of the THF^{2+} dication. In the calculations, out of 62 simulated trajectories, 40 resulted in the $H_2{}^+C_3H_5^+ + CHO^+$ channel without observation of the $H + H + C_3H_5^+ + CHO^+$ channel, indicating that the $H_2 + C_3H_5^+ + CHO^+$ channel is predominant in the dissociation process. The simulated KER is obtained by summing the kinetic energies of all products and the remaining Coulomb potential energy of two ions considering the center-of-mass distance. The calculated results from the AIMD simulations are displayed in Fig. 3(a) for comparison. The calculated KER values fall within the range of the experimental results,

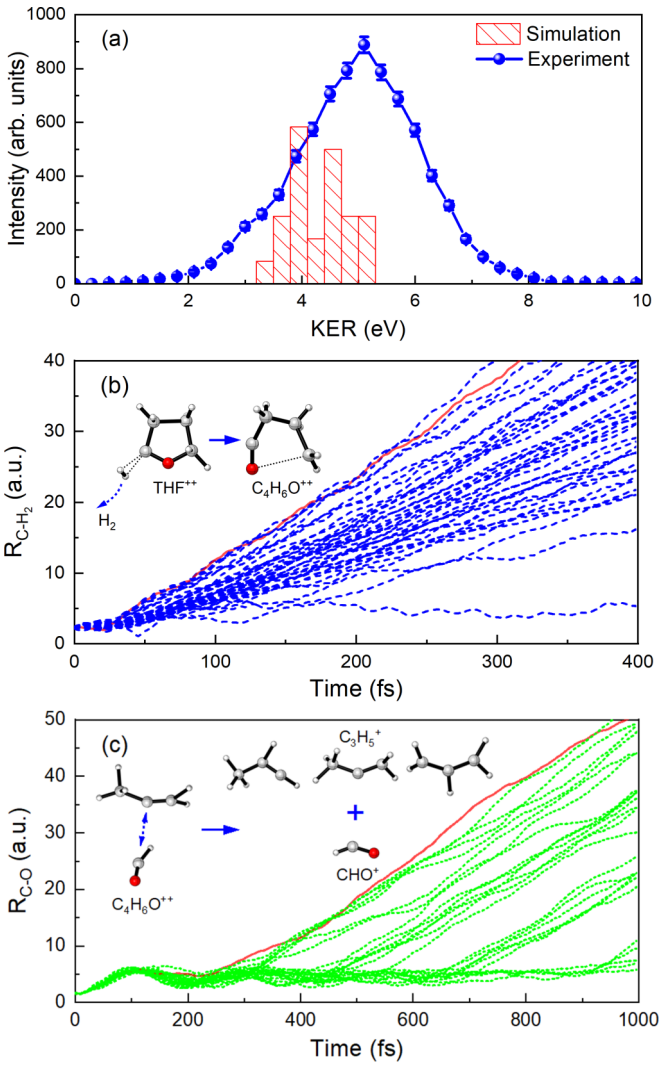

FIG. 3. (a) Experimental and simulated kinetic energy releases of the $H_2 + C_3H_5^+ + CHO^+$ channel. (b) Calculated fragment distances between H_2 and the remaining $C_4H_6O^{2+}$ as a function of time. (c) Calculated distances between $C_3H_5^+$ and CHO^+ fragments from the Coulomb explosion of $C_4H_6O^{2+}$ as a function of time. The blue dashed (upper) and green dotted (lower) lines originate from the same calculations, representing the H_2 ejection and ultimate separation into a $C_3H_5^+ + CHO^+$ ion pair, respectively. The red solid line represents a typical trajectory from the dynamical simulations, which has a shorter time for H_2 ejection and Coulomb explosion.

while its peak position is lower and its distribution width is narrower than the experimental results. The differences between calculated and experimental results can be attributed to the approximate calculations, where the fragmentation of excited states is approximated by introducing a quantified internal energy in the electronic ground state. Molecular-dynamics simulation methods capable of specifying excited states, such as the complete active space self-consistent field method [49], time-dependent density-functional theory [50,51], and nonadiabatic dynamics methods (such as the surface hopping model and dynamical surface Hamiltonian model [52]) are expected to bridge the current discrepancies between experimental and simulated results.

Figures 3(b) and 3(c) present the time-dependent fragmentation dynamics of the H_2 formation channel. The C–H_2 distance (R_{C-H_2}) represents the distance between the emitted H_2 and the residual $C_4H_6O^{2+}$ dication, confirming that the two dissociated hydrogen atoms combine to form molecular hydrogen H_2. The C–O distance (R_{C-O}) in Fig. 3(c) illustrates the CE separation of $C_3H_5^+$ and CHO^+ fragments over time. According to the AIMD results, the evolution of the H_2 formation channel $H_2 + C_3H_5^+ + CHO^+$ can be described as follows. In the first step, two hydrogen atoms, both from the same or different carbon sites, combine to form a hydrogen molecule. Different from the H_2 roaming, the forming H_2 molecule gains higher kinetic energy during the internal energy conversion process of the excited-state dication. The attraction between the H_2 molecule and the $C_4H_6O^{2+}$ ion is insufficient to bind them, resulting in the rapid escape of the H_2 molecule from the parent within roughly 50 fs. Following the ejection of H_2, the remaining five-membered-ring $C_4H_6O^{2+}$ dication undergoes an immediate ring-opening process via the C–O bonds breakage, forming a chainlike structure resembling $(OCCH_2CH_2CH_2)^{2+}$. This chainlike dication undergoes relaxation for approximately 300 fs and eventually breaks apart into a $C_3H_5^+ + CHO^+$ ion pair. The Coulombic repulsion between $C_3H_5^+$ and CHO^+ results in a monotonic increase in the distance between the two ions over time. Hydrogen migration occurs frequently during the relaxation processes of $C_4H_6O^{2+}$ dication and $C_3H_5^+$ cation, leading to structural rearrangements of these cations. Several possible $C_3H_5^+$ structures, such as CH_3CHCH^+, $CH_3CCH_2^+$, and $CH_2CHCH_2^+$, have been observed in the calculated time range (1000 fs).

To provide complementary information on the H_2 formation mechanisms and extend the results of the dynamical simulations, we performed high-level *ab initio* calculations on the PES of the THF^{2+} dication. As shown in Fig. 4, three types of H_2 formation pathways, following a scheme similar to that for the AIMD simulations, have been identified. These pathways can be classified by identifying the carbon site sources of H atoms in H_2, including both hydrogen atoms from the same *ortho*-carbon C_α of THF (named $H_\alpha H_\alpha$), from two different *meta*-carbons C_β of THF (named $H_\beta H_{\beta'}$), and from *ortho*- and *meta*-carbons of THF (named $H_\alpha H_\beta$). The relative energies and structures of reaction intermediates of three H_2 formation pathways are displayed in Figs. 4(a)–4(c).

The reaction pathways along the PES are in good agreement with the *ab initio* molecular-dynamics simulation results presented in Fig. 3. Upon double ionization of the THF molecule, the excited state of THF^{2+} can relax to the lowest-energy state of THF^{2+}, then rearrange significantly the molecular structure involving hydrogen migration and ring opening, and finally dissociate into $H_2 + C_3H_5^+ + CHO^+$. In the THF^{2+} dication, two hydrogen atoms originating from either the same or different carbon sites combine to form a H_2 molecule via a small barrier. Among the three pathways in Figs. 4(a)–4(c), the barrier (approximately 0.37 eV) of H_2 formation for the $H_\beta H_{\beta'}$ pathway is lowest, where the H atom initially connected at $C_{\beta'}$ transfers to C_β. The H_2 molecule, possessing sufficient energy, then escapes from the parent ion and becomes a free neutral molecule. After H_2 ejection, the remaining $C_4H_6O^{2+}$ dication forms a chain intermediate

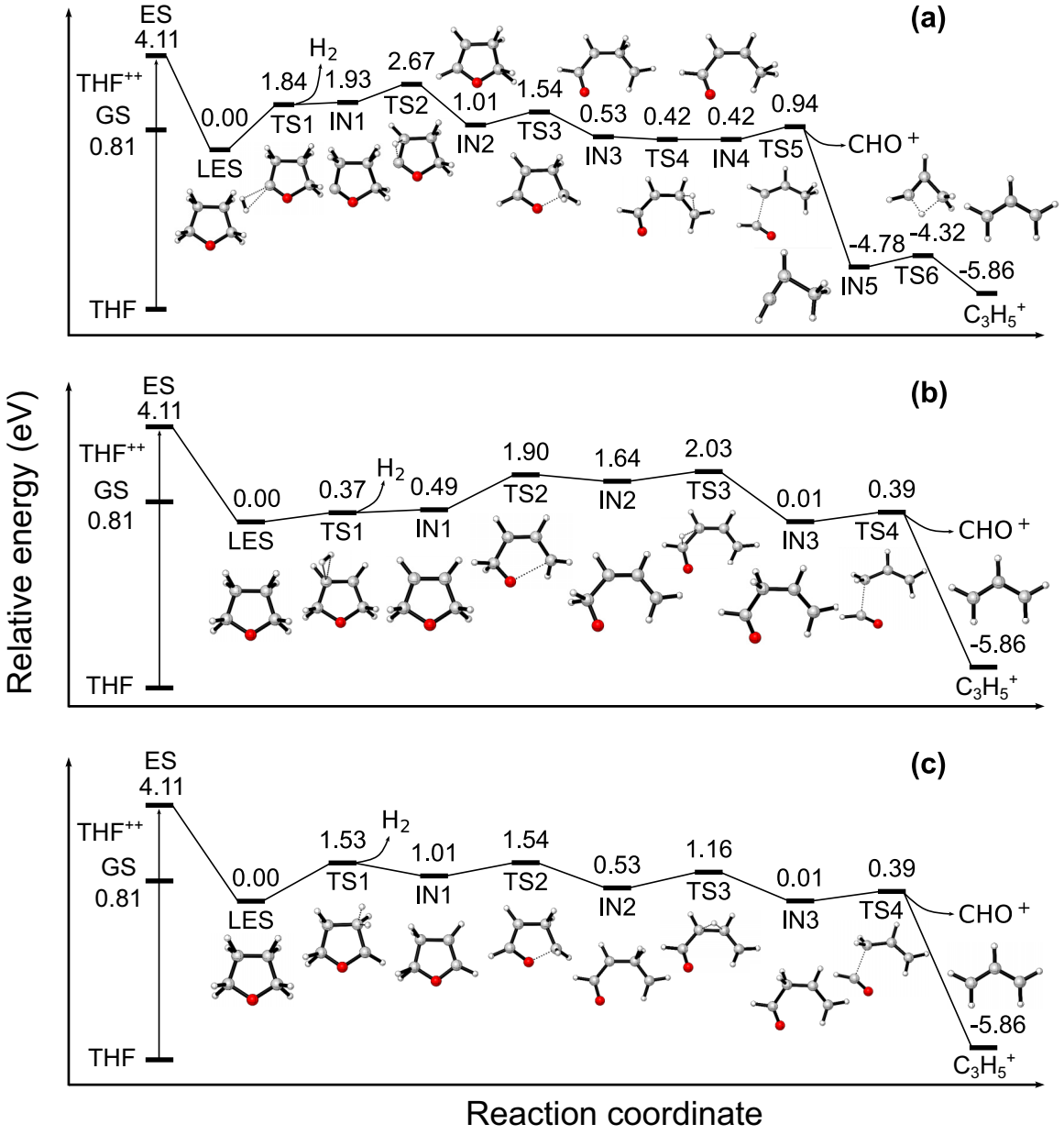

FIG. 4. Three possible reaction pathways with the selected transition states (TS) and intermediate states (IN) along the potential energy surfaces including both hydrogen atoms from (a) the same *ortho*-carbon C_α of THF (named $H_\alpha H_\alpha$), (b) two different *meta*-carbons C_β of THF (named $H_\beta H_{\beta'}$), and (c) *ortho*- and *meta*-carbons of THF (named $H_\alpha H_\beta$). The ground state (GS) corresponds to the ionization of two outermost valence electrons from THF. The population of the doubly ionized excited state (ES) initiates the H_2 formation channel studied here. The lowest-energy state (LES) of THF^{2+} is used as the reference point for energy calculations. The relative energies are given in eV. The three pathways are different at the hydrogen sources of the ejected H_2.

through a ring-opening process in which the C_α–O bond is broken. Here the $H_\alpha H_\alpha$ and $H_\alpha H_\beta$ pathways experience a small barrier during the ring-opening process (approximately 0.50 eV), whereas the $H_\beta H_{\beta'}$ pathway has a slightly larger barrier (approximately 1.0 eV). Subsequently, the breakage of the $C_{\alpha'}$–$C_{\beta'}$ bond leads to the complete breakage of the parent ions. Hydrogen migration occurs frequently with low barriers during the fragmentation processes, like TS4, TS3, and TS3 for $H_\alpha H_\alpha$, $H_\beta H_{\beta'}$, and $H_\alpha H_\beta$ pathways, respectively. This leads to the rearrangement of the molecular structure and eventually the formation of two charged products $C_3H_5^+ + CHO^+$. The structures of all possible reaction intermediate-, initial-, and final-state products, as well as the energy levels, have been determined. The final product structures are identified as H_2, $CH_2CHCH_2^+$, and HCO^+. The highest barriers of the rate-determining step of three H_2 formation pathways are 2.67 eV (TS2) for $H_\alpha H_\alpha$, 2.03 eV (TS3) for $H_\beta H_{\beta'}$, and 1.54 eV (TS2) for $H_\alpha H_\beta$ pathways, which mainly correspond to H migration and C–O bonds breakage. The energy of all intermediate states is lower than the energy of the initial

double-ionization state (the excited state), which is 3.3 eV higher than the dicationic ground state. This indicates that all three reaction pathways can proceed without barriers, forming the H_2, $C_3H_5^+$, and CHO^+ products. At the high excitation energy, this specific channel is independent of the barrier of the corresponding TS. Therefore, the three pathways should not be in competition but rather collectively promote the H_2 formation channel, potentially resulting in a broad distribution of the KER spectrum.

V. CONCLUSION

In summary, we have investigated the electron-collision-induced double ionization and subsequent dissociation of the THF molecule by combining multiparticle coincidence momentum measurements and *ab initio* calculations. The H_2 formation channel $H_2 + C_3H_5^+ + CHO^+$ was clearly defined, and the initial double-ionization state was determined by measuring the projectile energy-loss spectrum. The H_2 formation channel could be accessed by populating the double-ionization excited state with an energy 3.3 eV higher than the ground state (ionization of two outermost valence electrons). Further molecular-dynamics simulations indicated that the H_2 formation and ejection occur on an ultrafast timescale (approximately 50 fs), followed by the ring opening via the C–O bond cleavage and the ultimate Coulomb explosion. The PES calculations revealed several H_2 formation pathways, which are below the energy of the excited state and hence can proceed without barriers.

Since H_2 is the smallest and the most abundant interstellar molecule, its formation mechanism is of particular interest. The H_2 formation dynamics presented in this work can provide references to build accurate and realistic models for explaining the observed H_2 abundances in the diffuse ISM. Moreover, H_2 has been regarded as one of the ideal energy sources due to its carbon-free solutions [53]. However, the utilization of hydrogen to build a clean and sustainable energy system is constrained by key challenges in production and storage technologies [54]. Alicyclic compounds like THF, serving as liquid organic hydrogen carriers with high H content, present a promising method to store and produce H_2 [55]. Through the state-selective ionization techniques, it is possible to overcome the high-temperature requirement and reaction enthalpy for dehydrogenation of neutral molecules, thus providing a potential application for H_2 generation [56]. Our result are expected to stimulate the emergence of advanced technologies to realize efficient H_2 production.

ACKNOWLEDGMENTS

This work was jointly supported by the National Natural Science Foundation of China under Grants No. 12325406 and No. 92261201, the Shaanxi Province Natural Science Fundamental Research Project under Grant No. 2023JC-XJ-03, and the Shaanxi Fundamental Science Research Project for Mathematics and Physics under Grant No. 22JSY022.

[1] G. Vidali, H_2 formation on interstellar grains, Chem. Rev. **113**, 8762 (2013).

[2] S. E. Hosseini and M. A. Wahid, Hydrogen production from renewable and sustainable energy resources: Promising green energy carrier for clean development, Renew. Sust. Energ. Rev. **57**, 850 (2016).

[3] N. Ekanayake, T. Severt, M. Nairat, N. P. Weingartz, B. M. Farris, B. Kaderiya, P. Feizollah, B. Jochim, F. Ziaee, K. Borne, K. Raju P., K. D. Carnes, D. Rolles, A. Rudenko, B. G. Levine, J. E. Jackson, I. Ben-Itzhak, and M. Dantus, H_2 roaming chemistry and the formation of H_3^+ from organic molecules in strong laser fields, Nat. Commun. **9**, 5186 (2018).

[4] N. Ekanayake, M. Nairat, B. Kaderiya, P. Feizollah, B. Jochim, T. Severt, B. Berry, K. R. Pandiri, K. D. Carnes, S. Pathak, D. Rolles, A. Rudenko, I. Ben-Itzhak, C. A. Mancuso, B. S. Fales, J. E. Jackson, B. G. Levine, and M. Dantus, Mechanisms and time-resolved dynamics for trihydrogen cation (H_3^+) formation from organic molecules in strong laser fields, Sci. Rep. **7**, 4703 (2017).

[5] N. Ekanayake, M. Nairat, N. P. Weingartz, M. J. Michie, B. G. Levine, and M. Dantus, Substituent effects on H_3^+ formation via H_2 roaming mechanisms from organic molecules under strong-field photodissociation, J. Chem. Phys. **149**, 244310 (2018).

[6] E. Livshits, I. Luzon, K. Gope, R. Baer, and D. Strasser, Time-resolving the ultrafast H_2 roaming chemistry and H_3^+ formation using extreme-ultraviolet pulses, Commun. Chem. **3**, 49 (2020).

[7] E. Wang, X. Shan, L. Chen, T. Pfeifer, X. Chen, X. Ren, and A. Dorn, Ultrafast proton transfer dynamics on the repulsive potential of the ethanol dication: Roaming-mediated isomerization versus Coulomb explosion, J. Phys. Chem. A **124**, 2785 (2020).

[8] E. Wang, N. G. Kling, A. C. LaForge, R. Obaid, S. Pathak, S. Bhattacharyya, S. Meister, F. Trost, H. Lindenblatt, P. Schoch, M. Kübel, T. Pfeifer, A. Rudenko, S. Díaz-Tendero, F. Martín, R. Moshammer, D. Rolles, and N. Berrah, Ultrafast roaming mechanisms in ethanol probed by intense extreme ultraviolet free-electron laser radiation: Electron transfer versus proton transfer, J. Phys. Chem. Lett. **14**, 4372 (2023).

[9] K. Gope, E. Livshits, D. M. Bittner, R. Baer, and D. Strasser, An "inverse" harpoon mechanism, Sci. Adv. **8**, eabq8084 (2022).

[10] I. Luzon, E. Livshits, K. Gope, R. Baer, and D. Strasser, Making sense of Coulomb explosion imaging, J. Phys. Chem. Lett. **10**, 1361 (2019).

[11] K. A. Haupa, G. Tarczay, and Y.-P. Lee, Hydrogen abstraction/addition tunneling reactions elucidate the interstellar $H_2NCHO/HNCO$ ratio and H_2 formation, J. Am. Chem. Soc. **141**, 11614 (2019).

[12] A. Schneiker, S. Góbi, P. R. Joshi, G. Bazsó, Y.-P. Lee, and G. Tarczay, Non-energetic, low-temperature formation of C_α-glycyl radical, a potential interstellar precursor of natural amino acids, J. Phys. Chem. Lett. **12**, 6744 (2021).

[13] Y. Yang, H. Ren, M. Zhang, S. Zhou, X. Mu, X. Li, Z. Wang, K. Deng, M. Li, P. Ma, Z. Li, X. Hao, W. Li, J. Chen, C.

Wang, and D. Ding, H_2 formation via non-Born-Oppenheimer hydrogen migration in photoionized ethane, Nat. Commun. **14**, 4951 (2023).

[14] K. Gope, D. M. Bittner, and D. Strasser, Sequential mechanism in H_3^+ formation dynamics on the ethanol dication, Phys. Chem. Chem. Phys. **25**, 6979 (2023).

[15] A. M. Miksch, A. Riffelt, R. Oliveira, J. Kästner, and G. Molpeceres, Hydrogenation of small aromatic heterocycles at low temperatures, Mon. Not. R. Astron. Soc. **505**, 3157 (2021).

[16] A. Schneiker, G. Ragupathy, G. Bazsó, and G. Tarczay, Potential catalytic role of small heterocycles in interstellar H_2 formation: A laboratory astrochemistry study on furan and its hydrogenated forms, J. Phys. Chem. A **126**, 2832 (2022).

[17] T. Chen, M. Gatchell, M. H. Stockett, R. Delaunay, A. Domaracka, E. R. Micelotta, A. G. G. M. Tielens, P. Rousseau, L. Adoui, B. A. Huber, H. T. Schmidt, H. Cederquist, and H. Zettergren, Formation of H_2 from internally heated polycyclic aromatic hydrocarbons: Excitation energy dependence, J. Chem. Phys. **142**, 144305 (2015).

[18] C. Paris, M. Alcamí, F. Martín, and S. Díaz-Tendero, Multiple ionization and hydrogen loss from neutral and positively-charged coronene, J. Chem. Phys. **140**, 204307 (2014).

[19] R. Janečková, O. May, A. Milosavljević, and J. Fedor, Partial cross sections for dissociative electron attachment to tetrahydrofuran reveal a dynamics-driven rich fragmentation pattern, Int. J. Mass Spectrom. **365–366**, 163 (2014).

[20] C. Champion, M. A. Quinto, M. U. Bug, W. Y. Baek, and P. F. Weck, Theoretical and experimental quantification of doubly and singly differential cross sections for electron-induced ionization of isolated tetrahydrofuran molecules, Eur. Phys. J. D **68**, 205 (2014).

[21] E. Ali, X. Ren, A. Dorn, C. Ning, J. Colgan, and D. Madison, Experimental and theoretical triple-differential cross sections for tetrahydrofuran ionized by low-energy 26-eV-electron impact, Phys. Rev. A **93**, 062705 (2016).

[22] J. Zhou, E. Ali, M. Gong, S. Jia, Y. Li, Y. Wang, Z. Zhang, X. Xue, D. V. Fursa, I. Bray, X. Chen, D. Madison, A. Dorn, and X. Ren, Absolute triple differential cross sections for low-energy electron impact ionization of biochemically relevant systems: Water, tetrahydrofuran, and hydrated tetrahydrofuran, Phys. Rev. A **104**, 012817 (2021).

[23] W. Wolff, B. Rudek, L. A. da Silva, G. Hilgers, E. C. Montenegro, and M. G. P. Homem, Absolute ionization and dissociation cross sections of tetrahydrofuran: Fragmentation-ion production mechanisms, J. Chem. Phys. **151**, 064304 (2019).

[24] M. Dampc, E. Szymańska, B. Mielewska, and M. Zubek, Ionization and ionic fragmentation of tetrahydrofuran molecules by electron collisions, J. Phys. B: At. Mol. Opt. Phys. **44**, 055206 (2011).

[25] J. D. Builth-Williams, S. M. Bellm, L. Chiari, P. A. Thorn, D. B. Jones, H. Chaluvadi, D. H. Madison, C. G. Ning, B. Lohmann, G. B. da Silva, and M. J. Brunger, A dynamical (e,2e) investigation of the structurally related cyclic ethers tetrahydrofuran, tetrahydropyran, and 1,4-dioxane, J. Chem. Phys. **139**, 034306 (2013).

[26] X. Ren, T. Pflüger, M. Weyland, W. Y. Baek, H. Rabus, J. Ullrich, and A. Dorn, An (e, 2e + ion) study of low-energy electron-impact ionization and fragmentation of tetrahydrofuran with high mass and energy resolutions, J. Chem. Phys. **141**, 134314 (2014).

[27] X. Ren, E. Wang, A. D. Skitnevskaya, A. B. Trofimov, K. Gokhberg, and A. Dorn, Experimental evidence for ultrafast intermolecular relaxation processes in hydrated biomolecules, Nat. Phys. **14**, 1062 (2018).

[28] X. Xue, D. M. Mootheril, E. Ali, M. Gong, S. Jia, J. Zhou, E. Wang, J.-X. Li, X. Chen, D. Madison, A. Dorn, and X. Ren, Triple-differential cross sections in three-dimensional kinematics for electron-impact-ionization dynamics of tetrahydrofuran at 250-eV projectile energy, Phys. Rev. A **106**, 042803 (2022).

[29] E. Wang, X. Ren, W. Baek, H. Rabus, T. Pfeifer, and A. Dorn, Water acting as a catalyst for electron-driven molecular breakup of tetrahydrofuran, Nat. Commun. **11**, 2194 (2020).

[30] E. Wang, X. Ren, M. Gong, E. Ali, Z. Wang, C. Ma, D. Madison, X. Chen, and A. Dorn, Triple-differential cross sections for $(e, 2e)$ electron-impact ionization dynamics of tetrahydrofuran at low projectile energy, Phys. Rev. A **102**, 062813 (2020).

[31] E. Erdmann, M.-C. Bacchus-Montabonel, and M. Łabuda, Modelling charge transfer processes in C^{2+}–tetrahydrofuran collision for ion-induced radiation damage in dna building blocks, Phys. Chem. Chem. Phys. **19**, 19722 (2017).

[32] S.-H. Lee, Dynamics of multi-channel dissociation of tetrahydrofuran photoexcited at 193 nm: Distributions of kinetic energy, angular anisotropies and branching ratios, Phys. Chem. Chem. Phys. **12**, 2655 (2010).

[33] T. J. Wasowicz, A. Kivimäki, M. Dampc, M. Coreno, M. de Simone, and M. Zubek, Photofragmentation of tetrahydrofuran molecules in the vacuum-ultraviolet region via superexcited states studied by fluorescence spectroscopy, Phys. Rev. A **83**, 033411 (2011).

[34] D. Milešević, J. Stimson, D. Popat, P. Robertson, and C. Vallance, Photodissociation dynamics of tetrahydrofuran at 193 nm, Phys. Chem. Chem. Phys. **25**, 25322 (2023).

[35] J. Ullrich, R. Moshammer, A. Dorn, R. Dörner, L. Schmidt, and H. Schmidt-Böcking, Recoil-ion and electron momentum spectroscopy: Reaction-microscopes, Rep. Prog. Phys. **66**, 1463 (2003).

[36] R. Dörner, V. Mergel, O. Jagutzki, L. Spielberger, J. Ullrich, R. Moshammer, and H. Schmidt-Böcking, Cold target recoil ion momentum spectroscopy: A 'momentum microscope' to view atomic collision dynamics, Phys. Rep. **330**, 95 (2000).

[37] A. Dorn, M. Weyland, and X. Ren, Electron-ion momentum vector coincidences in electron collisions with atoms and molecules, J. Electron Spectrosc. Relat. Phenom. **230**, 33 (2019).

[38] S. Jia, J. Zhou, X. Wang, X. Xue, X. Hao, Q. Zeng, Y. Zhao, Z. Xu, A. Dorn, and X. Ren, Cold-target electron-ion-coincidence momentum-spectroscopy study of electron-impact single and double ionization of N_2 and O_2 molecules, Phys. Rev. A **107**, 032819 (2023).

[39] H. B. Schlegel, J. M. Millam, S. S. Iyengar, G. A. Voth, A. D. Daniels, G. E. Scuseria, and M. J. Frisch, *Ab initio* molecular dynamics: Propagating the density matrix with Gaussian orbitals, J. Chem. Phys. **114**, 9758 (2001).

[40] S. S. Iyengar, H. B. Schlegel, J. M. Millam, G. A. Voth, G. E. Scuseria, and M. J. Frisch, *Ab initio* molecular dynamics: Propagating the density matrix with Gaussian orbitals. II. Generalizations based on mass-weighting, idempotency, energy

conservation and choice of initial conditions, J. Chem. Phys. **115**, 10291 (2001).

[41] H. B. Schlegel, S. S. Iyengar, X. Li, J. M. Millam, G. A. Voth, G. E. Scuseria, and M. J. Frisch, *Ab initio* molecular dynamics: Propagating the density matrix with Gaussian orbitals. III. Comparison with Born–Oppenheimer dynamics, J. Chem. Phys. **117**, 8694 (2002).

[42] J. Zhou, S. Jia, X. Hu, E. Wang, X. Xue, Y. Wu, J. Wang, A. Dorn, and X. Ren, Intermolecular charge transfer induced fragmentation of formic acid dimers, Phys. Rev. Lett. **130**, 233001 (2023).

[43] K. Fukui, The path of chemical reactions—The IRC approach, Acc. Chem. Res. **14**, 363 (1981).

[44] M. Frisch, G. Trucks, H. Schlegel, G. Scuseria, M. Robb, J. Cheeseman, G. Scalmani, V. Barone, B. Mennucci, G. Petersson, H. Nakatsuji, M. Caricato, X. Li, H. Hratchian, A. Izmaylov, J. Bloino, G. Zheng, J. Sonnenberg, M. Hada, M. Ehara, K. Toyota *et al.*, *Gaussian 09* (Gaussian Inc., Wallingford, 2013).

[45] J. Rajput, T. Severt, B. Berry, B. Jochim, P. Feizollah, B. Kaderiya, M. Zohrabi, U. Ablikim, F. Ziaee, K. Raju P., D. Rolles, A. Rudenko, K. D. Carnes, B. D. Esry, and I. Ben-Itzhak, Native frames: Disentangling sequential from concerted three-body fragmentation, Phys. Rev. Lett. **120**, 103001 (2018).

[46] T. Yang, G. Su, C. Ning, J. Deng, F. Wang, S. Zhang, X. Ren, and Y. Huang, New diagnostic of the most populated conformer of tetrahydrofuran in the gas phase, J. Phys. Chem. A **111**, 4927 (2007).

[47] C. G. Ning, Y. R. Huang, S. F. Zhang, J. K. Deng, K. Liu, Z. H. Luo, and F. Wang, Experimental and theoretical electron momentum spectroscopic study of the valence electronic structure of tetrahydrofuran under pseudorotation, J. Phys. Chem. A **112**, 11078 (2008).

[48] P. Duffy, J. A. Sordo, and F. Wang, Valence orbital response to pseudorotation of tetrahydrofuran: A snapshot using dual space analysis, J. Chem. Phys. **128**, 125102 (2008).

[49] B. O. Roos, in *Advances in Chemical Physics*, edited by K. P. Lawley (Wiley, New York, 1987), Vol. 69, pp. 399–445.

[50] F. Furche and R. Ahlrichs, Adiabatic time-dependent density functional methods for excited state properties, J. Chem. Phys. **117**, 7433 (2002).

[51] J. Hutter, Excited state nuclear forces from the Tamm–Dancoff approximation to time-dependent density functional theory within the plane wave basis set framework, J. Chem. Phys. **118**, 3928 (2003).

[52] J. C. Tully, Molecular dynamics with electronic transitions, J. Chem. Phys. **93**, 1061 (1990).

[53] M. A. Rosen and S. Koohi-Fayegh, The prospects for hydrogen as an energy carrier: An overview of hydrogen energy and hydrogen energy systems, Energ. Ecol. Envir. **1**, 10 (2016).

[54] H. Ishaq, I. Dincer, and C. Crawford, A review on hydrogen production and utilization: Challenges and opportunities, in *SI: Progress in Hydrogen Production, Storage and Distribution*, edited by P. Ahmadi and N. Javani, special issue of Int. J. Hydrogen Energ. **47**, 26238 (2022).

[55] G. Sievi, D. Geburtig, T. Skeledzic, A. Bösmann, P. Preuster, O. Brummel, F. Waidhas, M. A. Montero, P. Khanipour, I. Katsounaros, J. Libuda, K. J. J. Mayrhofer, and P. Wasserscheid, Towards an efficient liquid organic hydrogen carrier fuel cell concept, Energ. Environ. Sci. **12**, 2305 (2019).

[56] M. R. Usman, Hydrogen storage methods: Review and current status, Renew. Sust. Energ. Rev. **167**, 112743 (2022).